



Nano gold coated hierarchically porous zinc titanium oxide sol-gel based thin film: fabrication and photoelectrochemical activity

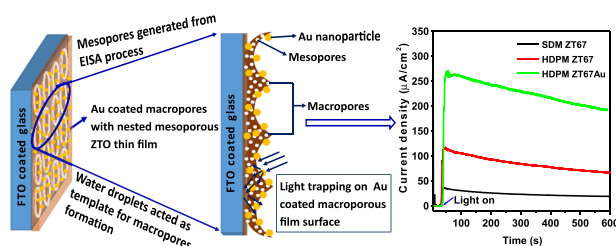
Hasmat Khan¹ · Malobi Seth¹ · Srikrishna Samanta¹ · Sunirmal Jana¹

Received: 11 May 2019 / Accepted: 1 August 2019 / Published online: 14 August 2019
© Springer Science+Business Media, LLC, part of Springer Nature 2019

Abstract

In this work, for the first time homogeneously distributed near periodic macroporous (HDPM) with nested mesoporous (hierarchically porous) semicrystalline zinc titanium oxide (ZTO) thin film on pure silica glass and fluorine doped tin oxide coated glass substrates was deposited by sol-gel dip coating technique from an optimized precursor solution of zinc nitrate hexahydrate and titanium isopropoxide with acetylacetonate in low boiling solvents. The HDPM film formation was carried out by simple breath figure method where the pore formation occurred from the generated water droplets via molecular condensation onto the as-deposited cold solution film surface owing to solvent evaporation. Zinc to titanium ratio in precursor solution, room relative humidity and other critical parameters were tailored towards optimization of the periodic macropores formation. Gold nanoparticles (NPs) were further deposited onto the ZTO thin films by solution technique. Crystallinity, surface morphology and microstructure of the thin films were critically analyzed by X-ray diffraction, atomic force, scanning, and transmission electron microscopic studies. The photoelectrochemical (PEC) performance of the films was examined under visible light irradiation. A significant improvement in PEC activity was observed in nano Au coated hierarchically porous thin film. This facile fabrication process could be applied in different mixed metal oxide thin films for improving the PEC activity of the materials.

Graphical Abstract



Nano gold coated periodic macro with nested mesoporous zinc titanium oxide sol-gel thin film with improved photoelectrochemical property

Supplementary information The online version of this article (<https://doi.org/10.1007/s10971-019-05108-x>) contains supplementary material, which is available to authorized users.

✉ Sunirmal Jana
sjana@cgcric.res.in

¹ Specialty Glass Technology Division, CSIR-Central Glass and Ceramic Research Institute (CSIR-CGCR), 196 Raja S.C. Mullick Road, Jadavpur, Kolkata, 700032 West Bengal, India

Highlights

- Fabricated periodic macro with nested mesoporous zinc titanium oxide (ZTO) thin film.
- The hierarchically porous (HP) ZTO film showed high BET surface area.
- Nano gold deposited HP film (NGHP) showed enhanced photoconversion efficiency.
- NGHP can have substantial opportunity in solar energy conversion.

Keywords Sol–gel thin films · Breath figure method · Metal oxide semiconductors · Hierarchically porous · Nano Au · Photoelectrochemical activity

1 Introduction

Because of rapid increase in global energy demand, development of advanced energy materials for efficient solar energy conversion is a challenging task for materials researchers. With the progressive consumption of fossil fuels as a conventional energy source, the necessity for development of the energy materials towards generation of alternative energy especially from solar light is thus increasing day by day. However, it is practically very difficult to utilize the solar energy efficiently and economically [1]. For this purpose, the conversion of solar energy into chemical energy via photoelectrochemical (PEC) water splitting technique has mostly been adopted [2]. In the recent times, the technique is greatly accepted to the researchers as it could be a promising one to fulfill both energy demand and environmental issues [1, 3]. A tremendous effort is going on globally to develop highly stable and efficient photoanode for enhancing the materials PEC performance where various factors such as surface to volume ratio and light harvesting capability of the electrode materials are greatly involved [4].

Metal oxide semiconductors (MOS) are highly promising photoanode materials which could effectively harvest solar light towards water oxidation reaction in PEC cells [5]. It is worthy to note that in PEC water oxidation, the semiconductor photoanode is the vital component. In this regard, various MOS, e.g., WO_3 , $\alpha\text{-Fe}_2\text{O}_3$, anatase TiO_2 , and BiVO_4 had mostly been used as photoanode materials [2]. Among these materials, the PEC activity of TiO_2 photoanode had been investigated extensively due to its availability, chemical inertness, and nontoxicity [6, 7]. However, the restricted light absorption ability of TiO_2 due to wide band gap (3.2 eV) limits its PEC performance [8]. It is also known that noble metal doping in large band gap semiconductor could increase the visible light absorption of TiO_2 [9]. Another way of enhancing the property of TiO_2 is to mix with other MOS like WO_3 , SnO_2 , and ZnO [2]. An ideal photoanode needs to maintain several tasks, e.g., light absorption/trapping, charge separation, and charge transport for efficient water decomposition. Moreover, the stability of the photoanode materials in aqueous solution is also one of the prime materials characteristics. A single MOS could not

fulfill all the tasks at a time. Thus, the study on photoanode with mixed metal oxide MOS has been started [10]. In the present work, ZnO as a low cost, easily available material with good optical and electrical property has been chosen with titanium oxide for the development of mixed metal oxide photoanode material.

On the other hand, the MOS based thin films with porous architecture have received greater interest in recent times for catalysis, photonics, enhanced light outcoupling for LEDs, light scattering and structural colors, reduced reflectivity especially in PEC application [2, 11]. Visible light absorption/trapping of MOS thin film could be increased by doping noble nano metal into the material [9]. In this respect, nano Au doping on the porous mixed metal oxide thin film could increase the light absorption via localized surface plasmon resonance (LSPR) effect in addition to help in charge separation during the PEC process [12].

Metal oxide thin films for the use as photoanodes could be deposited by different techniques such as electrodeposition, spray pyrolysis, drop-casting, anodization, chemical vapor deposition (CVD), magnetron sputtering, electron-beam evaporation, spin-coating or by using doctor blade. All these techniques are high cost and most difficult for large area fabrication whereas the sol–gel dip coating technique is one of the best ways to deposit homogeneous large area of coating [13]. In addition, several techniques had already been adopted for the fabrication of macroporous film, e.g., lithography, colloidal crystals, emulsion, and template processes. In this respect, breath figure method (BRF) is a simple, very fast, non-polluting and cost effective compared to the other processes [14]. It is also a promising approach for generation of regular sub-micrometer to micrometer sized periodic pore arrays in thin films [11]. In this process, self-organisation of water droplets arrays condenses onto the solution film surface due to evaporation of low boiling solvents from the film surface. The water droplet arrays act as templates for the pores. However, the BRF is widely used for generation of periodic macropores especially in organic polymer-based films [15]. It is rarely used in inorganic mixed MOS thin films [14]. Therefore, the work on the development of periodic macroporous MOS thin films via BRF method is found to be scanty in the literature [14, 16]. Previously, our group

already reported [14] the periodic macropore formation in zinc indium oxide thin film by the BRF method. In that work, it is seen that the formation of periodic macropores depends on various critical internal factors such as composition, viscosity, ageing time of precursor solution as well as external factors like room relative humidity during the thin film deposition. It is true that these factors might not simply be applicable in all the solution based mixed metal oxide thin film systems owing to change in chemistry of precursor solution [14]. Thus, more and more basic studies on different mixed metal oxide systems are primarily needed that would help to find out common critical factors as well as specific factors for a particular thin film system. Thus, one of the objectives of the present work is to enrich the knowledge-base with respect to zinc titanium oxide (ZTO) thin film system via BRF method. Other objectives of the work could be an examination of PEC activity of periodic macro with nested mesoporous ZTO thin film towards improvement in PEC activity by deposition of nano Au coating over the porous thin film.

In the present work, homogeneously distributed near periodic macroporous (HDPM) with nested mesoporous (hierarchically porous) ZTO sol–gel based thin film has been fabricated on pure silica/fluorine doped tin oxide coated glass substrate by BRF method. Critical parameters have been optimized towards formation of periodic macropores. By deposition of nano Au overlay coating; surface modification of the film for enhancing the PEC activity has also been performed. Morphological characterization of the films has been done by field emission scanning electron, atomic force, and transmission electron microscopes. In addition, the materials and optical properties of the thin film have also been characterized systematically. A detailed comparative study on microstructural, optical, textural, and visible light mediated PEC activity of periodic macroporous and scatterly distributed macroporous thin films fabricated by changing the room relative humidity has been performed in details. A significant improvement in PEC current density is observed in nano Au coated HDPM thin film.

2 Experimental

2.1 Precursor materials

Titanium isopropoxide (TIOP, Sigma Aldrich, assay $\geq 97\%$), zinc nitrate hexahydrate, (ZNH, Sigma-Aldrich), 2-butanol (Merck, assay $\geq 99\%$), methanol (Merck, assay $\geq 99\%$), ethanol (Emsure[®], ACS, ISO, Reagent, Ph Eur, Germany) and acetylacetone (acac, Merck, assay $\geq 98\%$), chloroauric acid (HAuCl_4 , SD Chemicals, 49%) were used as received without their further purifications for preparation of the precursor solutions.

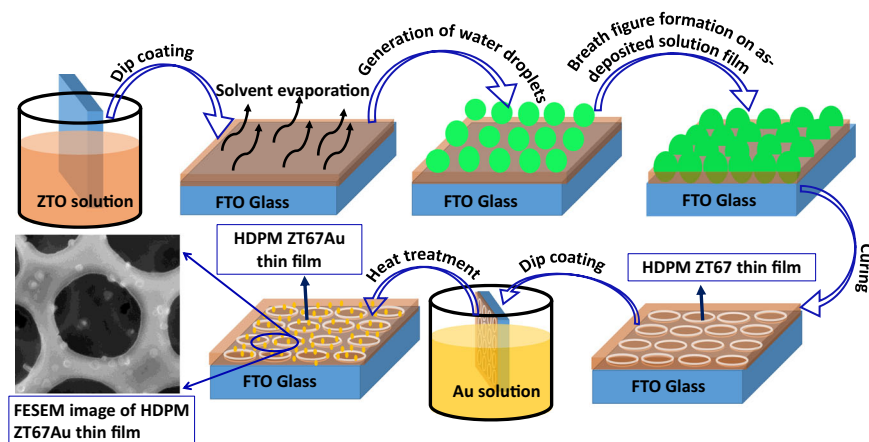
2.2 Preparation of precursor solutions

Initially, ZNH was added in ethanol and 2-butanol solvent mixture (1:1, w/w) and stirred the aliquot for 10 min with the help of a magnetic stirrer. After dissolving ZNH in the mixed solvent, a requisite amount of TIOP was added into the solution, followed by addition of acetylacetone (TIOP: acac = 1:1.5, molar ratio) as a solution stabilizing agent with further continuous stirring for about 24 h to obtain a clear homogeneous precursor solution for thin film formation. A series of precursor solutions were prepared where the atomic percentages of zinc with respect to titanium were 10, 20, 30, 40, 50, 60, 67, 70, 80, and 90. Accordingly, the solutions were designated as SZT10, SZT20, SZT30, SZT40, SZT50, SZT60, SZT67, SZT70, SZT80 and SZT90, respectively. Irrespective of the solution composition, total metal oxide content of the precursor solutions was kept fixed to 6 weight percent (wt.%). For a particular solution (SZT67), 4.38 g ZNH and 2.06 g TIOP were dissolved in the solvent mixture containing ethanol and 2-butanol (9 g of each) in presence of 1.08 g acetylacetone. In addition, a wide variation of ethanol content (0–100% with respect to 2-butanol) was made particularly in SZT67 solution, keeping fixed the TIOP to acac molar ratio and total metal oxide content in the precursor solution.

2.3 Film deposition

Deposition of zinc titanium oxide thin film was made by dip coating technique using Chemat Technology Inc., USA make Dip Master 200. The withdrawal speed of the substrate was varied from 15 to 20 cm/min to change the thickness of the film deposited onto glass substrates using an optimized ZTO precursor solution. Finally, the withdrawal speed was fixed at 18 cm/min to generate uniform coating onto the substrates. Pure silica glass (Quartz glass plate, code CUSQ223; Ants Ceramics Pvt. Ltd., India; dimension: length 75 mm, width 25 mm and thickness ~ 1 mm) as well as fluorine doped tin oxide (FTO; Product code- TISXZ 001; Techinstro, India; dimension: length 25 mm, width 25 mm, thickness 2.2 mm, and resistivity ~ 7 ohms/sq.) coated glass substrate was used for deposition of ZTO thin film. Before the film deposition, the substrates were cleaned by a known cleaning process reported in our previous work [14]. In brief, the substrates were washed with commercially available dilute soap solution and then, these were treated with ultra-sonication (Ultrasonic Cleaner, Piezo-U-Sonic, Sl. No. 100C). Finally, the cleaned substrates were washed by acetone followed by drying in an air oven. After dip coating, the as-coated glass substrates were kept for ~ 60 min in a clean room environment for generation of water droplets onto the solution film surface. For this purpose, a clean room (10,000+) was used where the room relative humidity (RH) could be controlled. During the film deposition

Fig. 1 Schematic diagram showing the fabrication of HDPM ZT67 and HDPM ZT67Au thin films on silica glass/FTO coated glass substrates



process, the RH and room temperature were maintained at 40–45% and 25 ± 3 °C, respectively. To remove the organics and waters in order to generate homogeneously distributed near periodic macropores with nested mesopores (hierarchically porous), the deposited films were thermally cured in an electrical oven under air atmosphere at 450 ± 5 °C with a heating rate of 1.5 °C/min and a soaking period of 4 h. The furnace was cooled down slowly to room temperature. The coated samples were designated as ZT10, ZT20, ZT30, ZT40, ZT50, ZT60, ZT67, ZT70, ZT80, and ZT90 according to the content of Zn (%) of 10, 20, 30, 40, 50, 60, 67, 70, 80, and 90 in the precursor solutions. The ZT67 film with scatterly distributed macropores (SDM was also prepared for comparison of particularly PEC activity of the ZT67 film having homogeneously distributed near periodic macropores (HDPM). For this reason, the as-coated solution film was immediately dried using an air drier to prevent the generation of water droplets onto the solution film surface and then, the sample was cured at 450 °C under the similar condition as adopted for the film with HDPM. On the other hand, for deposition of nano gold coating onto the ZTO thin films especially for HDPM ZT67, 0.04 M chloroauric acid (HAuCl_4) solution in methanol was used as Au precursor solution. Then, the as-coated HDPM ZT67 oxide film was further heat treated at 350 °C for about an hour in an electrical oven under an air atmosphere to obtain nano gold coated ZT67 thin film (HDPM ZT67Au). The overall film deposition including nano gold coating onto the HDPM ZT67 film is schematically displayed in Fig. 1.

3 Characterizations

3.1 Materials properties

To realize the crystallinity/crystal phase present in the ZTO thin films, grazing incidence X-ray diffraction (GIXRD) study was performed by employing Rigaku SmartLab, Japan make diffraction unit using $\text{CuK}\alpha$ radiation

(1.5406 Å) operating at 9 kW in the diffraction angle range (2θ) of 20° to 80°. A slit width of 5 mm was used for the XRD measurement. Optical microscopic images of the as-coated film were taken from an optical microscope (Olympus) to observe the presence of water droplets generated onto the solution film surface. Field emission scanning electron microscope (FESEM and FESEM-EDS, ZEISS, SUPRA™ 35VP) and atomic force microscope (AFM, Nanosurf Easy scan 2, Switzerland) were used to analyze the surface morphology/microstructure of the films. Transmission electron microscopic (TEM) measurement of the samples was done by FEI Company made (Tecnai G² 30STwin, Netherlands) machine at an accelerating voltage of 300 kV. Carbon coated 300 mesh Cu grids were used for placement of the samples. A Netzsch STA 409 C/CD thermo analyzer was used for thermo gravimetric analysis (TGA) using Al_2O_3 as a reference maintaining a fixed heating rate of 10K/min in air atmosphere. For the TGA run, the as-coated solution film (ZT67) was cured at 100 °C, then the material was scratched off to use for the measurement. A maximum temperature of 1000 °C was chosen. The FTIR spectral study (wavenumber range, 4000–400 cm^{-1}) was carried out by using Thermo Electron Corporation, USA make FTIR spectrometer (Nicolet 5700) with wavenumber accuracy ± 4 cm^{-1} . To evaluate surface area and pore size distribution in the film matrix, BET nitrogen adsorption–desorption isotherm was measured upon the scratched off ZTO thin film cured at 450 °C. The X-ray photoelectron spectra (XPS) of representative cured thin films, HDPM ZT67Au and SDM ZT67Au were measured with the help of PHI Versaprobe II Scanning XPS microprobe surface analysis system using $\text{Al-K}\alpha$ X-rays ($h\nu$, 1486.6 eV; ΔE , 0.7 eV at room temperature). The energy scale of the spectrometer was calibrated using pure Ag sample. The position of C1s peak was taken as standard with the binding energy of 284.5 eV. Light harvesting efficiency (LHE) of the thin films was also measured with the help of UV-Vis-NIR spectrophotometer (Shimadzu,

UV-3600) with an attachment of an integrating sphere (ISR-3100, UV-PC-3100).

3.2 PEC activity

PEC measurement of SDM ZT67, HDPM ZT67, and HDPM ZT67Au thin films deposited onto FTO coated glass substrate was performed with the help of Metrohm, Autolab AUt 85930 instrument using standard three-electrode cell under dark and visible-light exposure. For this purpose, a 300 W Xenon lamp with a water filter of 1 M NaNO₂ solution was used as the visible light (≥ 400 nm) source [14]. In this measurement, a Pt wire and an Ag/AgCl/3 M KCl electrode were taken as the counter electrode and reference electrode, respectively and ZTO thin film was used as the working electrode. An aqueous solution of 0.1 M KOH was used as an electrolyte. The chronoamperometric study (photocurrent density (PD) vs. time, I-t curve) of the thin films was carried out at 0.26 V vs. Ag/AgCl/3 M KCl [1.23 V vs. RHE, reversible hydrogen electrode].

4 Results and discussion

4.1 Phase structure

The crystallinity/crystal phase of ZTO thin films was analyzed with the help of GIXRD study. The XRD patterns (Fig. 2) of the samples confirmed that the thin films of pristine titanium oxide and zinc oxide were found to be crystallized at 450 °C curing temperature but in the mixed oxide thin films (e.g., HDPM ZT67), titanium oxide remained XRD amorphous up to 500 °C curing temperature.

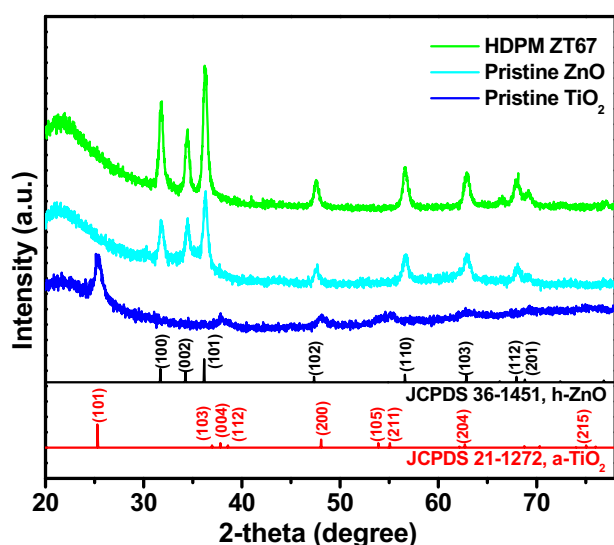


Fig. 2 XRD patterns of HDPM ZT67 as well as pristine zinc oxide and titanium oxide thin films cured at 450 °C. a-TiO₂ means anatase TiO₂

Generally, in zinc titanium oxide system, two intermediate compounds such as zinc ortho-titanate (Zn₂TiO₄) and zinc meta-titanate (ZnTiO₃) would crystallize [17] at relatively higher temperature (600–800 °C) [17, 18] compared to the curing temperature adopted for the present work. In this regard, the amorphous nature of titanium oxide in HDPM ZT67 thin film could be attributed due to incorporation of Zn(II) ions into titanium oxide network [19] and the excess Zn(II) ions present in ZT67 thin film matrix would crystallize to form hexagonal ZnO (h-ZnO). The substitution of titanium (IV) (size, ~0.06 nm) in titanium oxide matrix by Zn(II) ions (size, ~0.06 nm) would be favorable as both the ions are in similar size [19]. The XRD peaks with the 2θ (in degree) values of ~31.8, ~34.6, ~36.5, ~47.8, ~56.8, and ~62.8, confirmed the formation of hexagonal zinc oxide (h-ZnO) (JCPDS Card 36-1451) with the corresponding crystal planes of (100), (002), (101), (102), (110), and (103) (Fig. 2). It was important to note that the XRD patterns (ESM, Fig. S1) of ZT20, ZT30, ZT40, and ZT50 thin films were amorphous but ZT60 and ZT80 samples were XRD crystalline with the presence of h-ZnO at the curing temperature of 450 °C. In this case, the explanation regarding the amorphous nature of titanium oxide in ZT67 thin film could validate the above assumption. This was because up to Ti: Zn atomic ratio, 1:1, i.e., in the cases of ZT20, ZT30, ZT40 and ZT50 thin films, the thin film samples were XRD amorphous (ESM, Fig. S1). This could indicate that Zn(II) ions would fully be incorporated into the amorphous titanium oxide network [19].

4.2 Morphology and microstructure

4.2.1 Optical microscope study

Optical microscope image (Fig. 3a) of 30 min aged ZT67 solution film surface clearly showed the presence of spherical shaped water droplets. The water droplets would generate onto the solution film surface due to quick evaporation of volatile solvent at air-solution film interface [15]. After the generation of water droplets, these were stabilized to form breath figures (BRF) by polar groups such as nitrates. Subsequently, the BRF sank down into the solution film [15]. There were several key factors that could play the vital roles for the stabilization of BRF [14]. From the BRF, the nearly periodic macropores were found to form in the thin film after heat-treatment at 450 °C.

4.2.2 FESEM and AFM

FESEM and AFM studies were performed to observe the surface morphology of porous ZTO thin films. The FESEM image (Fig. 3) of the HDPM ZT67 thin film cured at 450 °C showed the presence of nearly uniform spherical macropores

Fig. 3 Surface morphology of as-coated film: **a** Optical microscope image; **b, c** FESEM images with different magnifications of zinc titanium oxide ZT67 thin film cured at 450 °C; **d, e** AFM images (two-dimensional, three-dimensional); **f** line scan profile obtained from (e) as indicated by arrow

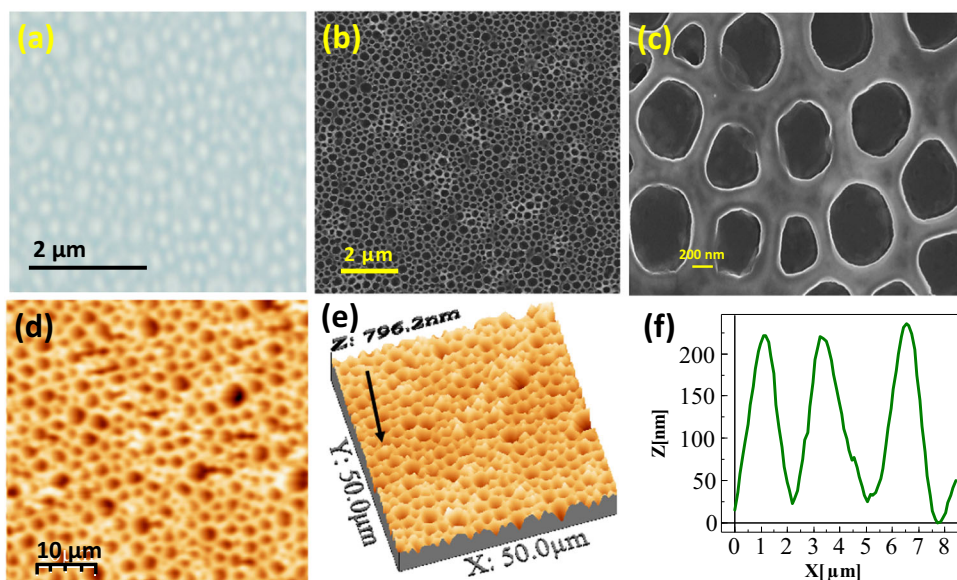
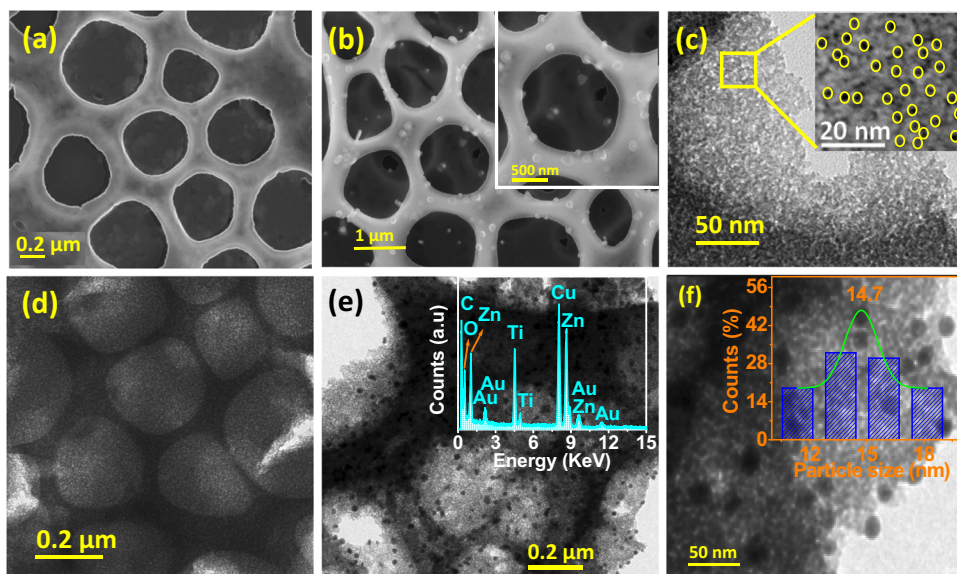


Fig. 4 FESEM images **a** HDPM ZT67 and **b** HDPM ZT67Au thin films cured at 450 °C. Inset of (b) represents a higher magnification FESEM image. TEM microstructural properties (c–f) of 450 °C ZT67 (c, d) and ZT67Au (e, f) thin films. Inset of (c) shows dark field TEM image taken from the selected area where the mesopores are shown by the black circles encircled in yellow color. Insets of (e, f) display the HDPM ZT67Au film TEM EDS plot and Au particle size distribution curve, respectively



with the pore diameter of 500–600 nm. The formation of macropores were also evident by TEM study (Fig. 4d, e; discussed later). On this aspect, the development of macropores with nested meso pores in indium zinc oxide system by BRF method had already been reported elsewhere by our group [14]. In this method, the water droplets are produced on solution (containing mixed solvents) film surface due to rapid evaporation of low boiling solvent from air-solution film interface and the high boiling solvent would help to sink down the water droplets into the solution film. Accordingly, the water droplets act as templates for the generation of nearly periodic macropores [16]. In the present work, the thin films (namely ZT10 to ZT90), the generation of the pores occurred only in the ZT30 to ZT70 samples. Among all the films only ZT67 film produced homogeneously distributed nearly

periodic macropores (HDPM) as clearly seen from the FESEM images (Fig. 3b, c) of the sample. This would arise owing to generation of metal (M/M') oxygen cross-linkages in mixed metal ions that could probably result in the formation of M–O–M' polymeric network in SZT67 solution (discussed details in Fig. S2, ESM). It is worthy to note that when zinc to titanium ratio was much lower i.e. in case of ZT10 and ZT20, no evidence of the macropores was found on the film surface of the samples (ESM, Fig. S3a, b). In fact, the macropores were started to appear in ZT30 film (ESM, Fig. S3c). In the case of lower content of zinc in the film (ZT10 and ZT20), the FESEM images showed nearly smooth film surface (ESM, Fig. S3a, b). This observation could relate to the presence of lower content of polymeric network formed in the precursor solution with relatively lower viscosity (2.96 cp and 3.16 cp

for the precursor solutions, SZT10 and SZT30, respectively). On the contrary, the system with higher zinc to titanium ratio particularly in ZT80 and ZT90 films derived from the precursor solutions of relatively higher viscosity (4.31 cp and 4.46 cp for the solutions SZT80 and SZT90, respectively), the SDM appeared as a consequence of lesser stabilization of self-organized water droplets onto the solution film with relatively high viscosity that would not help to sink down the water-droplets towards breath figure formation [14]. In addition, severe cracks were found on the film surface (ESM, Fig. S5a). The result could significantly support the above proposition of different content of polymeric network formation in the precursor solution that attributed to change in viscosity in the precursor solutions [14]. Viscosity (ESM, Table S2) and FTIR (ESM, Table S1, Fig. S2) spectral results of different precursor solutions for mixed oxide thin films are given in the electronic supplementary material (ESM). It was noted that the adequate water-droplets generation did not happen onto the as-coated solution films, ZT10 and ZT20 containing lower content of zinc in the precursor solutions. This observation clearly suggested that the macropores generation took place on the film surface due to the self-organized water droplets (BRF formation) [15]. The self-organization and stabilization of water droplets that act as template of the nearly periodic macropores would depend on various key factors like room relative humidity (RH), solution composition (zinc to titanium atomic ratio) and ethanol to 2-butanol weight ratio. The RH was kept at ~40–45% with fixing the ethanol to 2-butanol weight ratio, 1:1 for the formation of HDPM ZT67 film. The effect of solvent content on the formation of HDPM was also verified by FESEM analysis (ESM, Fig. S6a–d). The nano gold particles were observed in ZT67 film with HDPM (Fig. 4b). On the other hand, the AFM analysis (Fig. 3d, e) of HDPM ZT67 film was also performed to analyse the depth of the pores and root mean square (RMS) surface roughness. From the depth profile curve of AFM images, it was clearly seen that the pore depth was ~200 nm. The RMS surface roughness (ESM, Fig. S7a, b) values of SDM and HDPM films were ~50 nm and ~100 nm, respectively. It was further noted that after nano Au coating, the FESEM characterization for SDM ZT67Au sample was further performed (Fig. S8). Some SDM along with the presence of few numbers of Au nanoparticles were found to be embedded over the film. The size of nanoclusters of nano Au particles embedded over the ZT67 films was in the range of 30–40 nm for both the samples.

4.2.3 TEM study

TEM microstructural analysis of two representative samples, HDPM ZT67 and HDPM ZT67Au thin films was performed systematically. Figure 4 shows the TEM images of HDPM ZT67 and HDPM ZT67Au films. In the

FESEM image (Fig. 4b), the spherical shaped Au nanoparticles were clearly found to be decorated into the macropores. This observation was further confirmed from the corresponding bright field TEM image of scratched off HDPM ZT67Au film (Fig. 4e). The presence of mesopores in the film matrix was distinctly visible (Fig. 4c). The size of the mesopores was calculated from the selected area of dark field TEM image (inset, Fig. 4c) of the sample. It was seen that the calculated size of the mesopores was ~4 nm which was equivalent to pore size determined from the BET nitrogen adsorption–desorption isotherm measurement (Fig. 6, discussed later). The BET nitrogen adsorption–desorption isotherms confirmed the existence of slit-like mesopores in the film matrix. Moreover, the HRTEM (ESM, Fig. S9) result of the sample confirmed the presence of h-ZnO that fully corroborated the XRD result (Fig. 2) of HDPM ZT67 thin film. In HDPM ZT67Au thin film, the HRTEM image confirmed the presence of cubic Au nanoparticles and h-ZnO (ESM, Fig. S9a, c). Further, the existence of Au nanoparticles in HDPM ZT67Au film matrix was confirmed with the help of TEM EDX plot (inset, Fig. 4e). The size of Au nanoparticles was calculated from the bright field TEM image (Fig. 4f) of the sample. In this respect, the particle size distribution curve for Au nanoparticles (inset, Fig. 4f) showed ~15 nm average particle size of Au.

4.3 Thermogravimetric analysis and FTIR spectra

FTIR vibrations (Fig. 5b) of as-coated films showed the formation of metal complexes of acetylacetonate and nitrates. Two distinct FTIR peaks appeared ~1630 cm^{-1} and ~1392 cm^{-1} in the as-coated film were responsible for the stretching vibrations of metal complexes of acetylacetonate and free nitrate, respectively [13]. One broad peak appeared at ~3430 cm^{-1} , assigned to the vibration of hydroxyl groups present in the film [14]. These organics and nitrates of the as-coated film were found to be removed from the film matrix at the film curing temperature of 450 °C as evidenced from the disappearance of these FTIR vibrations. At this curing temperature, a broad band in the lower wavenumber region, 500–600 cm^{-1} was likely due to the vibration of the Ti–O bonds [20]. However, the vibrations within 430–450 cm^{-1} were responsible for the characteristic vibrations of Zn–O that present in ZnO of HDPM ZT67 thin film [21]. On the other hand, the FTIR study of the different solutions (SZT10, SZT30, SZT60, SZT67, SZT70, SZT80, and SZT90) was performed (ESM, Fig. S2) to understand the polymeric network formation in the precursor solution for mixed metal oxide film. In this respect, an intense stretching vibration was appeared at ~800 cm^{-1} in

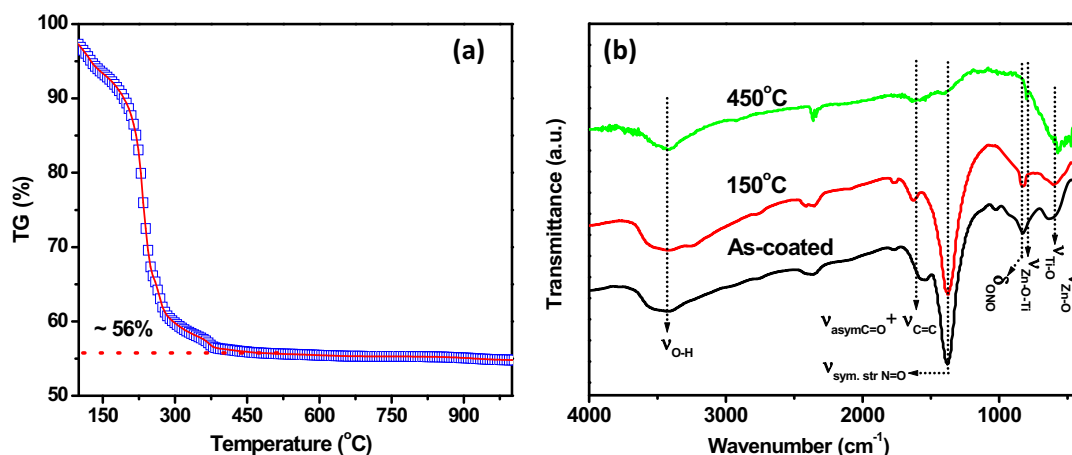
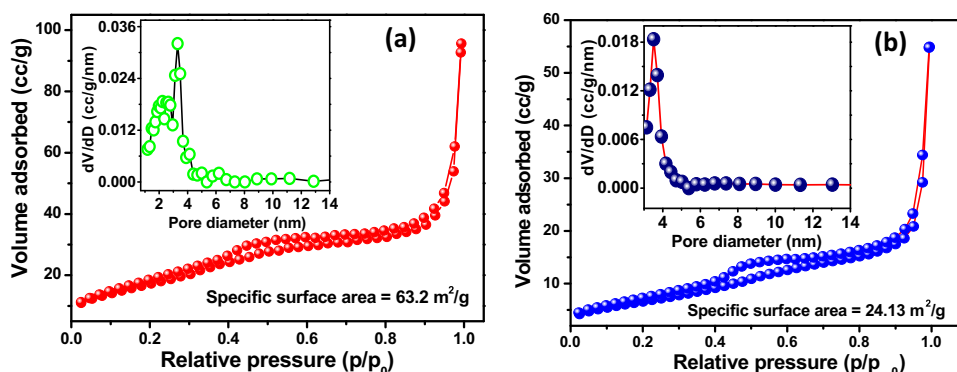


Fig. 5 **a** TGA curve of scratched off HDPM ZT67 gel film sample baked at 100 °C. **b** FTIR spectra of scratched off thin film sample baked at different temperatures as mentioned in the figure

Fig. 6 Adsorption–desorption isotherms of **a** scratched off thin films of HDPM ZT67 and **b** SDM ZT67, respectively. Insets of **a**, **b** are the respective pore size distribution curves of the films obtained from the desorption branch of the isotherms



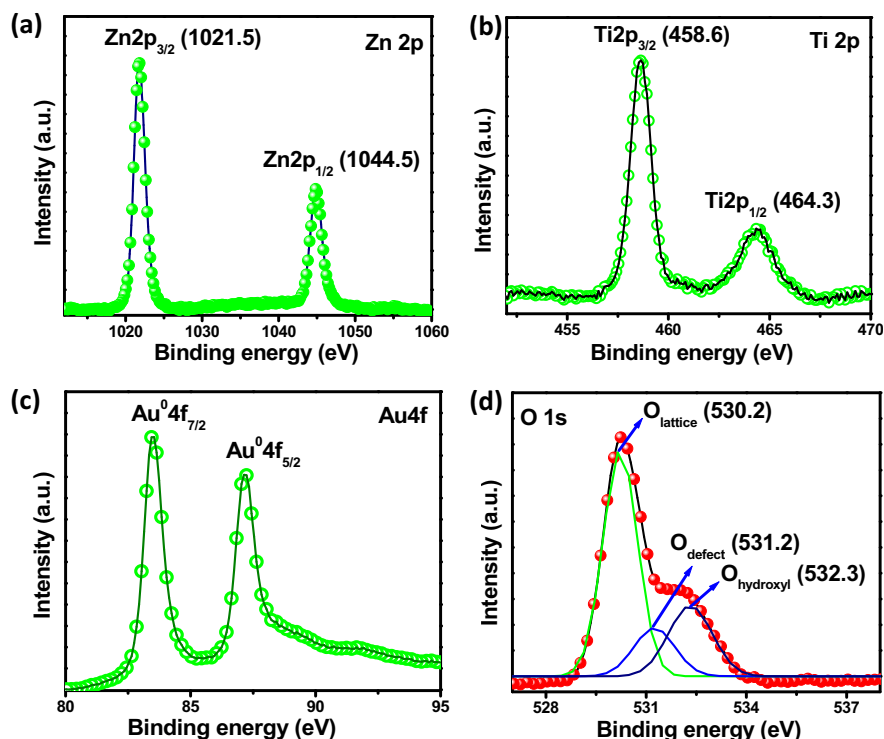
SZT67 sample (ESM, Fig. S2b). This stretching vibration could be attributed to Zn–O–Ti bond vibration [20]. It was seen that the highest intensity of the vibration (ESM, Fig. S2b) was observed in SZT67 solution, implying the formation of maximum content of polymeric network. Based on the FTIR spectral and viscosity measurements, it was realized that a polymeric structure with Zn–O–Ti bonding was formed in the optimized SZT67 precursor solution. The optimum concentration of this polymeric network in the solution might be responsible for the generation of HDPM thin films. The probable polymeric structure in the optimized SZT67 solution is displayed in Fig. S10 (ESM).

Effect of temperature on mass loss of the scratched off film matrix cured at 100 °C was obtained from thermogravimetric analysis (TGA, Fig. 5a). The TGA curve showed a gradual mass loss of the film materials with increasing the TG temperature. This loss of film materials could mainly be attributed to the presence of organics and nitrates as evidenced from the FTIR spectral study of the as-coated film (Fig. 5b). It was also seen that after 450 °C, the mass loss became negligible on further increasing the TG temperature. At 450 °C of TG temperature, an ~44% mass loss of the film materials was obtained.

4.4 Textural property

The textural properties of scratched off HDPM and SDM ZT67 thin film materials from BET nitrogen adsorption–desorption isotherm are shown in Fig. 6a, b. Both the isotherms highlighted IUPAC type IV architecture with H2 hysteresis loop, suggesting the films have an interconnected pore network [22]. The size of interconnected mesopores were calculated from the desorption branch of the isotherms. It was seen that the size of the mesopores were nearly same for both the films (~3.3 nm for HDPM film and ~3.5 nm for SDM film materials). This observation strongly supported the pore size data obtained from the dark field TEM image (inset, Fig. 4c) of the films. The BET specific surface area as obtained from the isotherm of HDPM ZT67 sample was ~63.2 m²/g. On the other hand, the SDM ZT67 film material showed much lower specific surface area (~24.1 m²/g) than the HDPM ZT67 film. This observation indicated the mesopores were found to be suppressed/decreased in SDM ZT67 film surface that might cause a decrease in the specific surface area of the film. In the SDM film matrix, most of the interconnected mesopores remained in blocked condition. However, in case of HDPM

Fig. 7 XPS binding energy curves of HDPM ZT67Au thin film: **a** Zn2p, **b** Ti2p, **c** Au4f, and **d** O1s



film, the blocked mesopores were observed to be uncovered due to the generation of periodic macroporous structure. As a consequence, the number of mesopores increased in HDPM film matrix. The enhancement of surface area over 2.6 times in HDPM than SDM is explained in Fig. S11 (ESM) where most of the interconnected mesopores in the thin film matrix would expose towards film-air interface. This situation would be compared with the fibrous roots of an anion (ESM, Fig. S11). It was worthy to note that the RMS surface roughness of HDPM ZT67 film was also two times higher than the SDM ZT67 thin film as measured by AFM study (ESM, Fig. S7). The macropores exposed within interconnected mesopores in the film matrix could provide a large numbers of active sites for superior electrolyte diffusion and mass transportation. The presence of homogeneously distributed nearly periodic macropores, HDPM could effectively harvest visible light towards the enhancement in PEC property of the thin film (discuss later).

4.5 XPS analysis

To investigate the oxidation states of constitute elements as well as the presence of oxygen defects/interaction of elements in ZTO thin film, the XPS analysis was thoroughly performed for a representative HDPM ZT67Au sample. In this respect, the existence of Zn^{2+} in the film was confirmed from the observation of strong binding energy peaks

(Fig. 7a) located at ~ 1044.5 and ~ 1021.5 eV, corresponded to the core levels of $Zn2p_{1/2}$ and $Zn2p_{3/2}$, respectively. The energy difference between the levels was found to be ~ 23.0 eV, confirming the zinc was in +2 oxidation state [23]. It was noted that the major oxidation state of titanium was revealed from the appearance of the binding energies of $Ti2p_{1/2}$ and $Ti2p_{3/2}$ core levels at ~ 464.3 and ~ 458.6 eV, respectively with their energy difference of ~ 5.7 eV (Fig. 7b) [24]. It was further noted that the strong binding energy peaks noticed at ~ 83.5 and 87.4 eV, indicated the existence of metallic gold with the core levels of $Au^0 4f_{7/2}$ and $Au^0 4f_{5/2}$, respectively (Fig. 7c). The binding energy values of $Au^0 4f_{7/2}$ and $Au^0 4f_{5/2}$ levels were also found to be slightly shifted to lower energies compared to the actual values of 84.0 and 87.7 eV, respectively [25]. This observation could suggest that a charge transfer happened between Au nanoparticles and zinc titanium oxide film matrix [25]. On the other hand, the binding energy peaks observed at ~ 530.2 , ~ 531.2 , and ~ 532.3 eV were the three Gaussian fitted peaks of O1s signal (Fig. 7d) of the sample. The peaks located at ~ 530.2 and ~ 531.2 eV corresponded to the lattice oxygen ($O_{lattice}$) and oxygen deficient region (O_{defect}), respectively [13]. However, the higher binding energy peak located at ~ 532.4 eV could relate to oxygen of hydroxyl group ($O_{hydroxyl}$) of the sample [13]. Furthermore, the XPS study of HDPM ZT67Au was compared with the SDM ZT67Au film to show the oxygen deficiency present in both the films. The calculated relative content (%) of $O_{lattice}$, O_{defect} and $O_{hydroxyl}$ were $\sim 57.1\%$,

~14.9% and ~28.1%, respectively in HDPM ZT67Au film matrix whereas, the calculated relative content (%) of O_{lattice} , O_{defect} and O_{hydroxyl} for SDM ZT67Au film were ~59.0%, ~10.1% and ~30.8%, respectively. Thus, the calculated content (%) of oxygen deficiency in the HDPM ZT67Au film matrix was ~1.5 times higher than the oxygen deficiency present in SDM ZT67Au film matrix (ESM, Fig. S12d). Thus, it is true that the presence of interaction between the Au nanoparticles with zinc titanium oxide matrix and the existence of oxygen defect in the film matrix would synergistically help to absorb more visible light towards enhancement of PEC properties [23] of the film (discussed later).

4.6 UV–visible absorption spectra

UV–visible absorption spectra of ZTO thin films with/without nano Au coating on silica glass substrate cured at 450 °C are shown in Fig. 8. The absorption spectra of ZTO films showed an absorption peak at ~360 nm due to the presence of ZnO semiconductor in the thin film matrix [26]. As already mentioned in the introduction section, the main objective of the present work is to create periodic macroporous structure towards maximizing visible light absorption by the thin film matrix through light diffraction and scattering phenomena. It is known that the incident light is diffracted and scattered in different directions by the periodic structures of a thin film [27]. The incident photons could reside into the thin film matrix for a prolonged time i.e., the optical path length of the incident light would be increased in the film matrix. As a result an enhancement in light absorption would occurred [28, 29]. In this work, the HDPM ZT67Au thin film (Fig. 8) showed a broad

absorption within the wavelength region of 400–500 nm. This absorption could be considered due to the coupling of propagating light with the resonant modes of periodic macropores of the thin film matrix [27–30]. The characteristic absorption peak of Au nanoparticles generally appears at the wavelength range 500–600 nm [25, 31]. Hence, it was true that the absorption peak shorter than 500 nm would not be due the LSPR of Au nanoparticles. It was due to the presence of periodic macroporous structure of the film. The low content of Au nanoparticles were found to be trapped onto the periodic macropores as evidenced from the TEM images (Fig. 4e, f) of the sample. In nano Au coated thin film (HDPM ZT67Au) an enhancement of absorption in the visible wavelength region was observed where the LSPR effect of Au nanoparticles is pronounced. This was because the visible absorption of the periodic macroporous film, i.e., the structural effect of the thin film surface was noticed in the broad wavelength region of 400–500 nm. Thus, the overall enhancement of visible absorption towards effective light harvesting in HDPM ZT67Au thin film was due to the synergistic effect of periodic macropores and LSPR of Au nanoparticles. In HDPM ZT67 sample, the interference pattern of light waves appeared generally due to an overlapping of electric fields generated by the incident photons into the periodic macropores of thin film semiconductor matrix [27–29, 32]. However, the absence of interference pattern in the UV–vis spectrum of SDM ZT67 thin film (Fig. 8) could attribute to the presence of SDM in the sample and hence, the SDM ZT67 thin film is found to behave planar in nature as evident from the surface microstructure by FESEM study (ESM, Fig. S8a). In this case, the incident light falls onto SDM ZT67 thin film surface and it might simply transmit without occurrence of light diffraction/scattering, i.e., no generation of interference of the incident light [33]. On the other hand, the light absorption particularly in the visible wavelength region enhanced after nano Au coating on HDPM ZT67 film surface. A broad absorption appeared at ~555 nm was observed in SDM ZT67Au film due to LSPR [29, 32] of Au nanoparticles (Fig. 8) but it was not clearly found in HDPM ZT67Au film. It is known that the surface plasmon polaritons (SSPs) form along the interface of a metal and a dielectric film [27, 34]. In the present work, LSPR and SPPs along with their hybridizations might provide an effective means towards enhancement in light absorption in the visible region [34, 35]. In this context, the interference formed due to homogeneously distributed periodic macropores, HDPM might be included within the enhanced visible absorption. Thus, the light absorption/harvesting in the visible region could be possible by periodic surface texturing by BRF method and noble metal overlay coating. This could surely improve the PEC activity of the thin film [23] (discussed later).

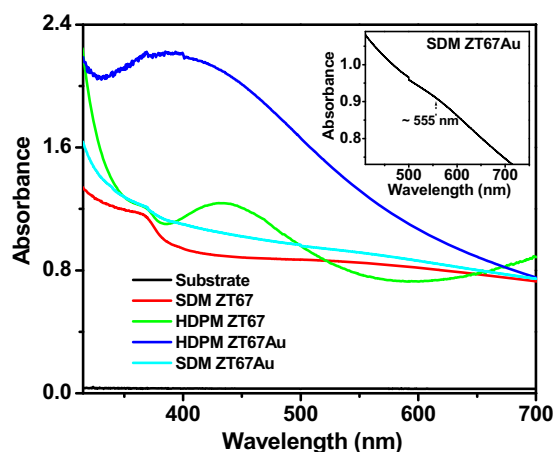


Fig. 8 UV–vis absorption spectra of ZTO films with/without nano Au coating. Inset displays the magnified absorption spectra of SDM ZT67Au thin film

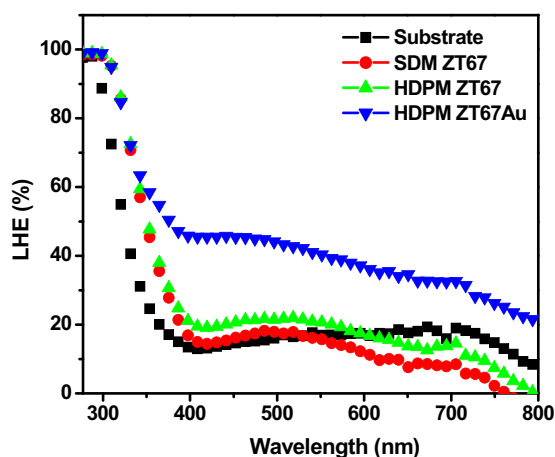


Fig. 9 Light harvesting efficiency of different thin film samples

4.7 Light harvesting efficiency (LHE)

The LHE of the SDM ZT67, HDPM ZT67, and HDPM ZT67Au thin films were evaluated (Fig. 9) using UV–vis spectral studies with the help of integrating sphere as a special attachment. It was to be noted that HDPM ZT67 film exhibited better LHE value compared to SDM ZT67 thin film. This observation could be associated with the presence of periodic macroporous structure which could increase the light absorption by photon trapping [13, 36]. However, the LHE increased significantly after nano Au coating on HDPM ZT67 film, i.e., in HDPM ZT67Au film. The presence of Au nanoparticles in the film matrix could enhance the light absorption due to LSPR effect as well as increasing effective optical path length of the incident light via multi-internal scattering [9, 36]. Thus, the nano Au coated HDPM ZT67 film could play a key role for improving the LHE value (Eq. 1) [28, 36]. The strategy could be used to make an efficient photoanode with enhanced PEC activity.

$$\text{LHE}(\lambda)(\%) = 100\% - R(\lambda)(\%) - T(\lambda)(\%) \quad (1)$$

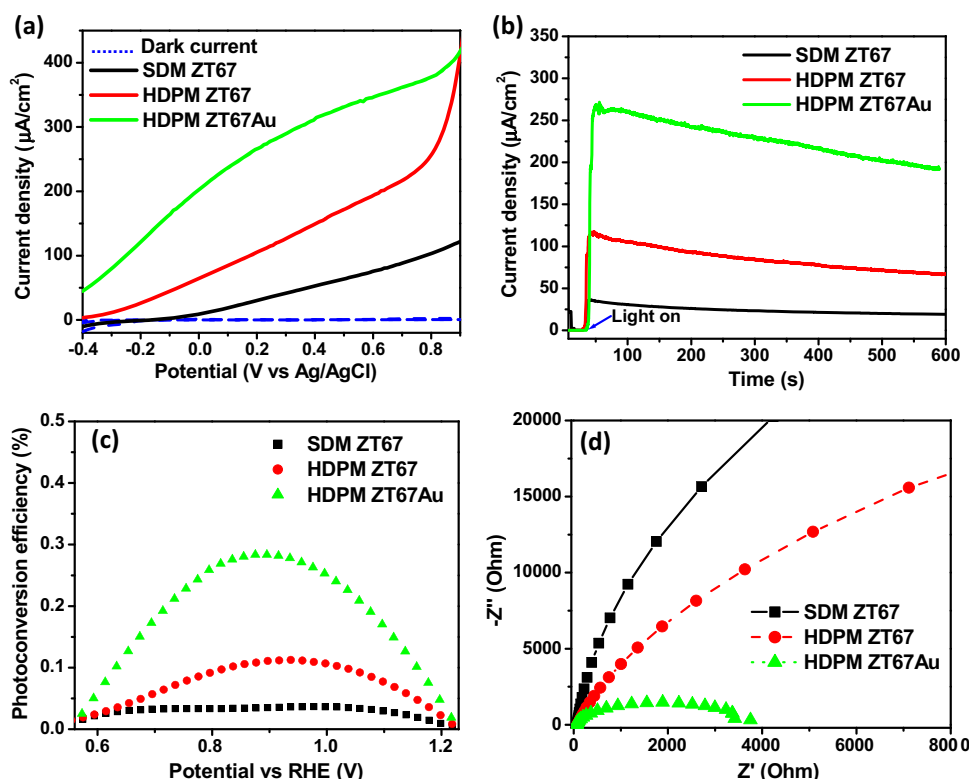
where R and T denote reflection and transmission, respectively.

4.8 PEC activity

To examine the PEC performance of macroporous ZTO thin films especially HDPM ZT67 with/without nano Au coating and SDM ZT67 thin film under visible light irradiation, all the films were deposited onto a commercially available conducting fluorine doped tin oxide (FTO) coated glass substrate used as photoanode. The ZT67 thin film with SDM was also coated on FTO coated glass substrate for comparison. However, in case of ZT67 thin film with SDM, the deposition and thermal curing process was different as stated in details under experimental section. It was worthy to note that the PEC activity (Fig. 10) of the films was investigated using three-

electrode systems in 0.1 M KOH solution. The linear sweep voltagrams (LSV, Fig. 10a) of ZTO films was measured in the range of -0.4 to 0.8 V vs. Ag/AgCl/3 M KCl reference electrode under illumination of visible light (wavelengths, ≥ 400 nm) [14] of the xenon lamp source (with a water filter of 1 M NaNO₂ solution) as well as in dark condition (Fig. 10a). Upon the visible light exposure, a significant increase in anodic PD in HDPM ZT67 film was observed compared to other films. The LSV curve of the ZT67 film with SDM showed (Fig. 10a) lower PD compared to HDPM ZT67 thin film. This could be possible due to the presence of periodical macroporous structure that could enhance the surface area as well as light harvesting/trapping ability via increasing the optical path length of incident light of the film as already evidenced from the measurement of BET nitrogen adsorption–desorption isotherm and UV–vis spectra, respectively [30]. Homogeneously distributed periodic macroporous ZT67 film absorbed more visible light than scatterly distributed macroporous ZT67 film (Fig. 8). It could also enhance the PD under visible light irradiation [37]. Moreover, the RMS surface roughness was found to be much higher in periodic macroporous film than scatterly distributed macroporous film. The higher surface area could provide more active sites for electrolyte diffusion and mass transportation [13, 23]. The electrochemical impedance spectra (EIS) were also measured for all the samples to confirm the charge separation and transportation occurred in ZTO films. It was noted that the arc radii of EIS Nyquist plots (Fig. 10d) of the films revealed an interface layer resistance occurring at the surface of the samples [23]. It was also observed that the arc radius of the EIS plot of HDPM ZT67 thin film was much smaller than the SDM ZT67 film, confirming that an efficient photogenerated charge separation took place in HDPM ZT67 photoanode. This result implied an improvement in photogenerated charge separation and transportation occurred in HDPM ZT67 film during the PEC process. In this context, a significant visible light trapping/absorption occurred in HDPM ZT67 film as evident from the measurement of the optical properties of the films (Fig. 8). The periodic macroporous film could increase the optical path length of light that significantly improved the light absorption ability [38] vis-à-vis enhancing the PEC activity [14]. It is also known that the PEC activity depends on microstructure of the thin film matrix. The mesoporous microstructure (Fig. 4c) of HDPM ZT67 film with higher surface area could provide large number of active sites for ionic diffusion and mass transportation [23]. Improvement in PD with comparable long term photostability was found in the I-t curve (Fig. 10b) of HDPM ZT67 film under visible light exposure. Moreover, the LSV curve of HDPM ZT67Au film showed ~ 2.4 times higher PD than HDPM ZT67 film (with respect to RHE as obtained from Eq. 2). This observation could be attributed to the presence of LSPR effect of metallic Au NPs with a facile charge

Fig. 10 PEC activities of ZTO films: **a** Linear sweep voltammetry (LSV) curves measured under illumination of visible light and dark (blue dashed line) conditions. **b** Change of current density with time (*I*-*t* curves) of different ZTO films recorded under visible light exposure. **c** Applied bias photon-to-current conversion efficiency curves of ZTO films calculated from their corresponding LSV curves. **d** EIS Nyquist plots of the ZTO photoanodes under visible light exposure



separation occurred in HDPM ZT67Au film [38]. The applied bias photon-to-current efficiency (ABPE) η of the films were calculated from their corresponding LSV curves by using Eq. 3 [39]. All the applied potentials reported in efficiency curve were converted to RHE scale from Ag/AgCl electrode using Nernst equation (Eq. 2).

$$E_{\text{RHE}} = E_{\text{Ag/AgCl}} + 0.059 \text{ V} \times \text{pH} + E_{\text{Ag/AgCl}}^{\circ} \quad (2)$$

$$E_{\text{Ag/AgCl}}^{\circ} = 0.1976 \text{ V vs. NHE at } 25^{\circ}\text{C}$$

$$\eta = J(1.23 - V_{\text{app}}) / P_{\text{in}} \times 100\% \quad (3)$$

where J is the measured photocurrent density; V_{app} is the measured applied voltage; P_{in} is the intensity of the illuminated light in mW/cm^2 .

5 Conclusion

In brief, near periodic macro with nested mesoporous (hierarchically porous) semicrystalline zinc titanium oxide (ZTO) sol-gel based thin film was fabricated by BRF method. Several critical parameters including zinc to titanium ratio in precursor solution, room relative humidity were tailored towards optimization of the periodic macropore formation. Gold nanoparticles (NPs) were further deposited onto the hierarchically porous film by solution

technique. Crystallinity, surface morphology and microstructure of the thin films were critically analyzed by X-ray diffraction, atomic force, scanning and transmission electron microscopic studies. The PEC performance of the films was examined under visible light irradiation. A significant improvement in PEC activity was observed in Au NPs coated periodic macroporous thin film. This facile fabrication process could be applied in other mixed metal oxide thin films for improving the PEC activity of the materials.

Acknowledgements One of the authors, HK thankfully acknowledges CSIR, Govt. of India for providing his Ph.D. research fellowship. The authors also acknowledge the help rendered by Electron Microscopy Section for XRD, FESEM, and TEM characterizations. The work had been done as an associated research work of 12th Five Year Plan project of CSIR (No. ESC0202).

Compliance with ethical standards

Conflict of interest The authors declare that they have no conflict of interest.

Publisher's note: Springer Nature remains neutral with regard to jurisdictional claims in published maps and institutional affiliations.

References

1. Cho S, Jang J-W, Lee K-H, Lee JS (2014) Research update: strategies for efficient photoelectrochemical water splitting using metal oxide photoanodes. *Appl Mater* 2:1–14

2. Kang D, Kim TW, Kubota SR, Cardiel AC, Cha HG, Choi K-S (2015) Electrochemical synthesis of photoelectrodes and catalysts for use in solar water splitting. *Chem Rev* 115:12839–12887
3. Yang J-S, Wu J-J (2018) Toward eco-friendly and highly efficient solar water splitting using $\text{In}_2\text{S}_3/\text{anatase/rutile TiO}_2$ dual-staggered-heterojunction nanodendrite array photoanode. *ACS Appl Mater Interfaces* 10:3714–3722
4. Ji M, Cai J, Ma Y, Qi L (2016) Controlled growth of ferrihydrite branched nanosheet arrays and their transformation to hematite nanosheet arrays for photoelectrochemical water splitting. *ACS Appl Mater Interfaces* 8:3651–3660
5. Nguyen O, Krins N, Laberty-Robert C (2018) Harvesting light with semiconductor: role of interface in the processes of charge transfer. *Mater Sci Semicond Process* 73:2–12
6. Cao F, Xiong J, Wu F, Liu Q, Shi Z, Yu Y, Wang X, Li L (2016) Enhanced photoelectrochemical performance from rationally designed anatase/rutile TiO_2 heterostructures. *ACS Appl Mater Interfaces* 8:12239–12245
7. Fujishima A, Zhang X, Tryk DA (2008) TiO_2 photocatalysis and related surface phenomena. *Surf Sci Rep* 63:515–582
8. Kwiatkowski M, Bezverkhyy I, Skompska M (2015) ZnO nanorods covered with a TiO_2 layer: simple sol–gel preparation, and optical, photocatalytic and photoelectrochemical properties. *J Mater Chem A* 3:12748–12760
9. Upadhyay AP, Behara DK, Sharma GP, Gyanprakash M, Pala RGS, Sivakumar S (2016) Fabricating appropriate band-edge-staggered heterosemiconductors with optically activated Au nanoparticles via click chemistry for photoelectrochemical water splitting. *ACS Sustain Chem Eng* 4:4511–4520
10. Krol RVD, Grätzel M, (2012) *Electronic Materials: Science & Technology*, in: Krol RVD, Grätzel M (Eds) *Photoelectrochemical Hydrogen Production*. Springer, New York, p. 9
11. Kon K, Brauer CN, Hidaka K, Lohmannsroben H-G, Karthaus O (2010) Preparation of patterned zinc oxide films by breath figure templating. *Langmuir* 26:12173–12176
12. Pandikumar A, Murugesan S, Ramaraj R (2010) Functionalized silicate sol-gel-supported TiO_2 -Au core-shell nanomaterials and their photoelectrocatalytic activity. *ACS Appl Mater Interfaces* 2:1912–1917
13. Khan H, Bera S, Sarkar S, Jana S (2017) Fabrication, structural evaluation, optical and photoelectrochemical properties of soft lithography based 1D/2D surface patterned indium titanium oxide sol-gel thin film. *Surf Coat Technol* 328:410–419
14. Bera S, Pal M, Sarkar S, Jana S (2017) Hierarchically structured macro with nested mesoporous zinc indium oxide conducting film. *ACS Appl Mater Interfaces* 9:4420–4424
15. Ding J, Zhang A, Bai H, Li L, Lia J, Ma Z (2013) Breath figure in non-aqueous vapor. *Soft Matter* 9:506–514
16. Li H, Jia Y, Du M, Fei J, Zhao J, Cui Y, Li J (2013) Self-organization of honeycomb-like porous TiO_2 films by means of the breath-figure method for surface modification of titanium implants. *Chem Eur J* 19:5306–5313
17. García-Ramírez E, Mondragón-Chaparro M, Zelaya-Angel O (2012) Band gap coupling in photocatalytic activity in ZnO– TiO_2 thin films. *Appl Phys A* 108:291–297
18. Arin J, Thongtem S, Phuruangrat A, Thongtem T (2017) Template synthesis of Zn_2TiO_4 and $\text{Zn}_2\text{Ti}_3\text{O}_8$ nanorods by hydrothermal calcination combined processes. *Mater Lett* 193:270–273
19. Pérez-González M, Tomás SA, Morales-Luna M, Arvizu MA, Tellez-Cruz MM (2015) Optical, structural, and morphological properties of photocatalytic TiO_2 -ZnO thin films synthesized by the sol-gel process. *Thin Solid Films* 594:304–309
20. Moradi S, Azar PA, Farshid SR, Khorrami SA, Givianrad MH (2012) Effect of additives on characterization and photocatalytic activity of TiO_2/ZnO nanocomposite prepared via sol-gel process. *Int J Chem Eng* 2012:1–5
21. Naskar A, Khan H, Bera S, Jana S (2017) Soft chemical synthesis, characterization and interaction of ZnO graphene nanocomposite with bovine serum albumin protein. *J Mol Liq* 237:113–119
22. Sangwichien C, Aranovich GL, Donohue MD (2002) Density functional theory predictions of adsorption isotherms with hysteresis loops. *Colloids Surf A Physicochem Eng Asp* 206:313–320
23. Bera S, Khan H, Biswas I, Jana S (2016) Polyaniline hybridized surface defective ZnO nanorods with long-term stable photoelectrochemical activity. *Appl Surf Sci* 383:165–176
24. Khan H, Seth M, Naskar A, Jana S (2018) Nano gold-coated surface patterned mesoporous titanium tin oxide sol–gel thin film: fabrication, optical and photoelectrochemical properties. *J Sol-Gel Sci Technol* 88:359–370
25. Zhang SW, Zhang BP, Li S, Li XY, Huang ZC (2016) SPR enhanced photocatalytic properties of Au-dispersed amorphous BaTiO_3 nanocomposite thin films. *J Alloy Compd* 654:112–119
26. Naskar A, Khan H, Sarkar R, Kumar S, Halder D, Jana S (2018) Anti-biofilm activity and food packaging application of room temperature solution process based polyethylene glycol capped Ag-ZnO-graphene nanocomposite. *Mater Sci Eng C* 91:743–753
27. Yang X, Zhou S, Wang D, He J, Zhou J, Li X, Gao P, Ye J (2015) Light Trapping Enhancement in a Thin Film with 2D Conformal Periodic Hexagonal Arrays. *Nanoscale Res Lett* 284(10):1–9
28. Jiang W, Liu H, Yin L, Shi Y, Chen B (2016) Enhanced photoelectric properties in dye-sensitized solar cells using TiO_2 pyramid arrays. *J Phys Chem C* 120:9678–9684
29. Leung S-F, Zhang Q, Xiu F, Yu D, Ho JC, Li D, Fan Z (2014) Light management with nanostructures for optoelectronic devices. *J Phys Chem Lett* 5:1479–1495
30. Wooh S, Yoon H, Jung J-H, Lee Y-G, Jai HK, Lee B, Kang YS, Char K (2013) Efficient light harvesting with micropatterned 3D pyramidal photoanodes in dye-sensitized solar cells. *Adv Mater* 25:3111–3116
31. Dunklin RJ, Forcherio TG, Roper DK (2015) Gold nanoparticle-polydimethylsiloxane films reflect light internally by optical diffraction and Mie scattering. *Mater Res Express* 2(085005):1–19
32. Sarkar S, Chattopadhyay R, Jana S (2016) Structural and light coupling characteristics of patterned silica-titania sol–gel thin films with/without nano gold coatings. *RSC Adv* 6:109218–109233
33. Bi Y-G, Feng J, Ji J-H, Yi F-S, Li Y-F, Liu Y-F, Zhang X-L, Sun H-B (2018) Nanostructures induced light harvesting enhancement in organic photovoltaics. *Nanophotonics* 7(2):371–391
34. Luo X, Tsai D, Gu M, Hong M (2019) Extraordinary optical fields in nanostructures: from sub-diffraction-limited optics to sensing and energy conversion. *Chem Soc Rev* 48:2458–2494
35. Kim J, Koh JK, Kim B, Kim JH, Kim E (2012) Nanopatterning of mesoporous inorganic oxide films for efficient light harvesting of dye-sensitized solar cells. *Angew Chem Int Ed* 51:6864–6869
36. Zhou L, Zhao C, Giri B, Allen P, Xu X, Joshi H, Fan Y, Titova LV, Rao PM (2016) High light absorption and charge separation efficiency at low applied voltage from Sb-doped $\text{SnO}_2/\text{BiVO}_4$ core/shell nanorod-array photoanodes. *Nano Lett* 16:3463–3474
37. Mayer J, Gallinet B, Offermans T, Ferrini R (2015) Diffractive nanostructures for enhanced light-harvesting in organic photovoltaic devices. *Opt Express* 24:358–373
38. Kumar DR, Manoj D, Santhanalakshmi J (2014) Au–ZnO bullet-like heterodimer nanoparticles: synthesis and use for enhanced nonenzymatic electrochemical determination of glucose. *RSC Adv* 4:8943–8952
39. Xu Y-F, Rao H-S, Wang X-D, Chen H-Y, Kuang D-B, Su C-Y (2016) In situ formation of zinc ferrite modified Al-doped ZnO nanowire arrays for solar water splitting. *J Mater Chem A* 4:5124–5129